JTTEE5 5:317-334

Technology of Thermally Sprayed Anilox Rolls: State of Art, Problems, and Perspectives

L. Pawlowski

This paper deals with the surfacing technology of ceramic anilox rolls. The rolls are used in the printing industry to transport the precisely determined quantity of ink in the flexographic printing machines. The technology of roll surfacing is discussed by taking the following aspects into account: preparation of the powder to spray the ceramic coating; thermal spraying of the duplex (bond coating and ceramic top coating); postspray finishing by grinding and polishing; and laser engraving. The powder used as the top coating of the aniloxes is chromium oxide. This powder might be prepared by such techniques as agglomeration, fusing, and crushing, etc. The preparation technique influences coating properties, such as microstructure (tested with SEM, OM, XRD, and XPS), open porosity, microhardness, and modulus of elasticity. Comparison of these properties enables optimum powder preparation techniques to be found. APS technique is used to coat the anilox rolls. Optimization of the plasma spraying parameters is discussed. Aniloxes are submitted to the grinding and polishing of the ceramic coating before laser engraving occurs. The final roughness of the finished coating is discussed in view of an optimum absorption of the laser light energy at engraving. Possible ways of reducing the spraying time are discussed, and future research toward improving the anilox roll quality is proposed.

Nomenclature

A	powder production technique by agglomeration (spray drying)
AD	powder production technique by agglomeration and subsequent densification
APS	atmospheric plasma spraying
AR	anilox rolls
AS	arc spraying
C	powder production technique enabling crystalline particles to be obtained
CTE	coefficient of thermal expansion
FC	powder production technique by fusing and crushing
FS	flame spraying
HEPS	high energy plasma spraying
HVOF	high-velocity oxygen fuel
HV	Vickers microhardness
IPS	inert plasma spraying
LD	line density
MIP	mercury intrusion porosimeter
NA	powder of NiAl
NC	powder of NiCr
OM	optical microscope
q	powder feed rate
R_z	coefficient describing roughness
SC	powder production technique by sintering and crushing
SEM	scanning electron microscope
SPS	shrouded plasma spraying
VPS	vacuum plasma spraying
XPS	x-ray photoelectron spectroscopy
XRD	x-ray diffraction

L. Pawlowski, Université d'Artois, Faculté des Sciences Appliquées, Laboratoire Laser-Plasma-Matériaux, Technoparc Futura, F-62400 Béthune, France.

Keywords anilox rolls, microstructure of Cr_2O_3 coatings, plasma spraying of ceramics, properties of Cr_2O_3 coatings

1. Introduction

ANILOX rolls (AR) used in flexographic machines started to be coated with ceramic plasma sprayed coatings about 10 years ago. Apart from thermal spraying, the AR surfacing technology includes mechanical grinding and polishing and laser engraving. The greatest difficulty results from the diversity of technological processes coming from the distant fields of the surfacing, mechanical, and optical engineering.

The present review is based on professional records of the author, available catalogs of the workshops producing AR, and discussions with the experts working in the field.

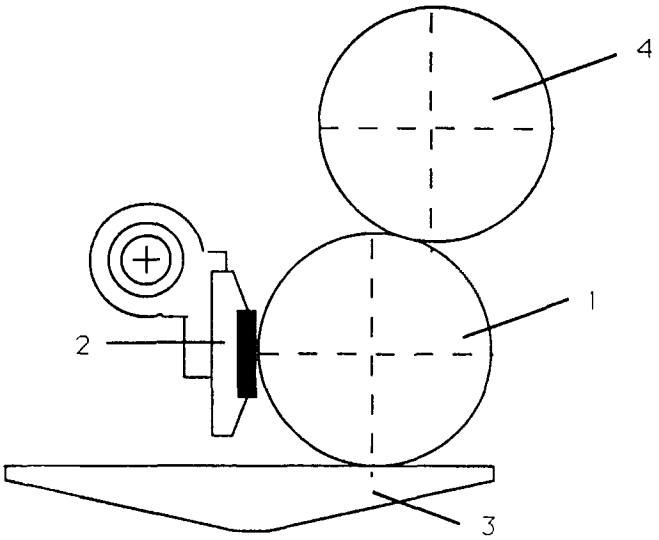

Fig. 1 Part of a flexographic printing machine: 1, anilox roll; 2 doctor blade; 3, ink container; 4, printing roll

The anilox rolls are used in printing machines working in the flexographic system (see Fig. 1). The roll (1), being in contact with a doctor blade (2), transports the precisely defined quantity of ink from the ink container (3) onto the printing roll (4).The used inks are water or solvent based and have different viscosities (depending on the solid content in the ink varying from 25 to 50 vol%).The quantity of the transported ink is determined by depth and density of the cell engraved in the roll surface. Excessive ink is removed by the doctor blade or the doctor roll. A typical roll is shown in Fig. 2.

The prior conventional technology of AR includes galvanic deposition of copper or nickel bond coating, followed by mechanical engraving with diamond indenters, and finally, the galvanic deposition of a wear-resistant chromium top coating. Modern rolls are ceramic with plasma sprayed chromium oxide top coating deposited onto a metallic bond coat. The top coating is ground and polished, engraved with a laser, and polished prior to service. The quality of the ceramic top coating is decisive in the AR quality in service. The properties of this coating are specified in Table 1 (Ref 1).

Table 1 A preliminary specification for the ceramic top coating of anilox rolls

No.	Coating property	Property specification	Remarks
1	Open and interconnected porosity	Low (<5%)	To prevent ink penetration to the bond coat and metallic roll
2	Pores size	Small (less than half of cell diameter; 15 μm for ruling 300 lines/cm)	To prevent ink accumulation inside the cells
3	Hardness	HV greater than 1000	To promote wear resistance
4	Cohesion	High Young modulus, high toughness	To promote coatings integrity
5	Homogeneity (inclusions of suboxides or metal)	Homogeneous	To avoid possible interaction with water-based inks
6	Light absorption	High light absorption	For the wavelength 10.6 μm (CO_2 laser)

The specified properties could be fulfilled by a plasma sprayed alumina coating. However, alumina becomes translucent after laser engraving, and it is impossible to make the microscopic measurements of the depth of the engraved cells. Another possible coating, for example alumina titania alloy, interacts with some printing inks (Ref 2). Finally, the chromium oxide coating is used and discussed in this paper.

2. Materials

2.1 *Roll*

New rolls are presently made of stainless steel. The older, refurbished ones are made of lower grade steels that corrode in contact with water-based inks. The concentricity of the roll must be at least 0.02 mm, and the roll must be well balanced. The weight of the roll ranges from a few hundred to several thousand kilograms.

2.2 *Powders (Wires) for Bond Coatings*

The bond coating should fulfill two functions: protect the substrate against corrosion (thus the coating should be dense and of corrosion-resistant material) and enhance adhesion of the ceramic top coating to the substrate.

The dense metallic coatings should be sprayed using any technique having a protective atmosphere, such as vacuum plasma spraying (VPS), inert plasma spraying (IPS), or shrouded plasma spraying (SPS) (see Ref 3). Most ARs have large dimensions that make it difficult to handle in any chamber (as in the VPS and IPS techniques). The SPS technique still remains a possibility. On the other hand, application of arc spraying (AS) or flame spraying (FS) wire techniques would lower production costs. However, the quality of coatings sprayed using these techniques is not very high; therefore, the APS technique is used to spray the metallic coatings.

The coatings might be sprayed using Ni or nickel alloys, such as NiCr or NiAl. In spray practice, the coarse powders are used if well-adhering bond coatings are expected. The fine powders are used if a high coating density is aimed. Thus a compromise is necessary to obtain well-adhering and dense deposits. A possible compromise consists of spraying the coarse powder (hav-

Table 2 Some properties of chromium oxide powders manufactured by different techniques used to spray top coatings of anilox rolls

Powder description	Powder type	Particle size, μm d_{10}	d_{50}	d_{90}	Chemical composition, wt%	Particle morphology	Apparent density, g/cm³
FC	FC	18.1	30.4	50.2	Bal. Cr_2O_3, 0.04 SiO_2, 0.04 TiO_2, 0.03 Fe_2O_3, 0.01 Cr-soluble	Blocky regular (Fig. 3a)	2.42
SC1	SC	20.8	32.9	49 0	Bal. Cr_2O_3, 4.15 SiO_2, 2.96 TiO_2, 0.01 Fe_2O_3, 0.01 Cr-soluble	Blocky irregular slightly rounded (Fig. 3b)	2.03
A1	A	14.3	31.2	67.9	Bal Cr_2O_3, 5 SiO_2, 0.01 Fe_2O_3	Hollow spheres and spheres (Fig. 3c)	1.22
A2	A	5 9	9.8	16.2	Bal. Cr_2O_3, 5 SiO_2, 0 01 Fe_2O_3	Hollow spheres and spheres	1.18
SC2	SC	37.1	73.7	37.1	Bal. Cr_2O_3, 5 SiO_2, 3 TiO_2	Blocky irregular (Fig. 3e)	2.22
C	C	4.4	7.4	12.4	Cr_2O_3	Crystalline (Fig. 3f)	2.53

Note: FC is fused and crushed, SC is sintered and crushed, A is spray-dried (agglomerated), and C is crystalline. d_{10}, d_{50}, d_{90} are the diameters corresponding to 10, 50, and 90% on the cumulative plot obtained with particle sizer Chemical composition data were given by the manufacturers. Apparent density was determined following ASTM B212.

ing sizes in the range of –90 to +45 μm) directly on the substrate and then applying a few layers of the fine powder (for example, particle sizes in the range of –45 to +5.6 μm). (A layer is a coating deposited in one pass of the torch over the substrate.)

In this study, the commercially available powder of Ni + 20 wt% Cr (NC) of particle size –90 to +45 μm (for example, Amperit 252.2 from Herman C. Starck Berlin, Germany) was used to spray the bond coatings. This powder, having particle sizes in the range –45 to +5.6 μm (Amperit 251.3), was also applied to spray the composites between the bond and the top coatings. The NC powder was produced by the water atomizing technique.

The Ni + 5 wt% Al powder of particle sizes in the range of –88 to +45 μm (NA) produced by the porous cladding technique (see Ref 3) by Sulzer-Metco, Wohlen, Switzerland (powder tradename is METCO 450) was also used to spray the bond coatings.

2.3 *Powders for Top Coatings*

At present, the chromium oxide powders, containing eventually small quantities of silicon oxide and/or titanium oxide, are used to spray top coatings.

Titanium oxide is frequently alloyed with other oxides to lower slightly the melting point. Thermal spraying of such a powder results in a higher quantity of melted particles than spraying of the pure oxide. Melting of the sprayed particles is in turn a prerequisite to obtaining coatings of desired low values of open and interconnected porosity (see Table 1). On the other hand, the silicon oxide acts as a glass former. In fact, melting of Cr_2O_3-5 wt%SiO_2 starts at about 2000 K with the melting of silica that coexists with solid chromium oxide (Ref 4). The lamellae that have the composition and temperature after the impact would contain liquid silicon oxide. Liquid SiO_2 could fill the pores generated at the impact of the particles. Thus this additive could also contribute to lowering the porosity of the coating.

The powders discussed here are, in part, commercially available. They were prepared using the following techniques (described in details in Ref 3): fusing and crushing (FC), sintering and crushing (SC), and crystallizing (C). (The technology of crystallizing enables the particles consisting of well-defined crystals to be formed. The Cr_2O_3 powder produced by this technology is manufactured by S.T. Praxair, Indianapolis, IN, USA, under tradename CRO-131.)

The chromium oxide powders produced using SC and FC (high-temperature techniques) are sometimes slightly substoichiometric (Ref 5). Plasma spraying of substoichiometric powders might result in the coating containing inclusions of metallic chromium (see Table 1). Therefore, a low-temperature powder production technique was also applied. This technique consists of mixing the fine pigments of Cr_2O_3 and SiO_2 with 50 wt% water and organic binder to obtain a slurry. The slurry was spray dried at about 490 K (Ref 4) to obtain an agglomerated A powder. Two batches of this powder with different sizes A2 (fine) and A1 (coarse) have been screened out. A part of the latter one was submitted to densification in an argon arc plasma (powder A1D).

Some properties of the powders are collected in Table 2. The powders are of three sizes: coarse with a d_{50} of about 70 μm (powder SC2), "regular" with a d_{50} of about 30 μm (powders FC, SC1, A1), and fine with a d_{50} of about 10 μm (powders A1, C). The morphology of these powders is presented in Fig. 3.

The particles of agglomerated A1 and A2 powders contain many fine pores (see Fig. 3c). Some particles exhibit internal holes that might arise from the presence of air occluded in the slurry used to spray dry (Ref 6). The densification of agglomerated powder eliminates the fine pores but does not eliminate the holes (see Fig. 3d). The FC and C particles are dense (see Fig. 3a and f), which is also confirmed by their high apparent density (see Table 2). On the other hand, sintered and crushed powders SC1 and SC2 of chromia with silica and titania, commercialized by two different manufacturers, have similar chemical composition but different internal morphology. Some of the SC1 powder particles contain inclusions (presumably of silica or titania) that are not visible in the SC2 powder particles. This suggests that the sintering of SC1 powder was carried out at a different temperature than that of SC2 powder as confirmed by the difference in the apparent densities of the powders.

Table 3 Quantitative XPS analysis and the atomic ratios of the chromium oxide powders manufactured using different techniques

Powder type	Element concentration, at.%					Atomic ratio	
	Cr	O	C	Si	Na	Cr/Si	Cr/O
FC	28.3	57.2	14.5	...	..	...	0.49
SC1	24.2	59.1	5.0	9.5	2.2	2.5	0.41
A1	8.6	45.0	37.3	2.9	6.2	2.9	0.19

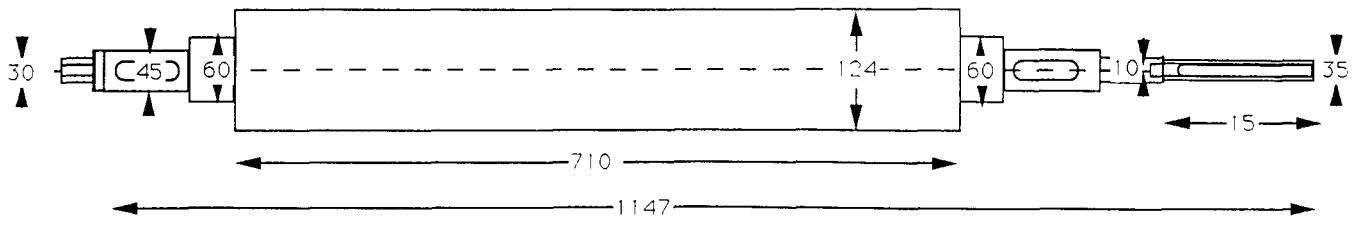

Fig. 2 Sketch of a typical anilox roll (all dimensions in millimeters)

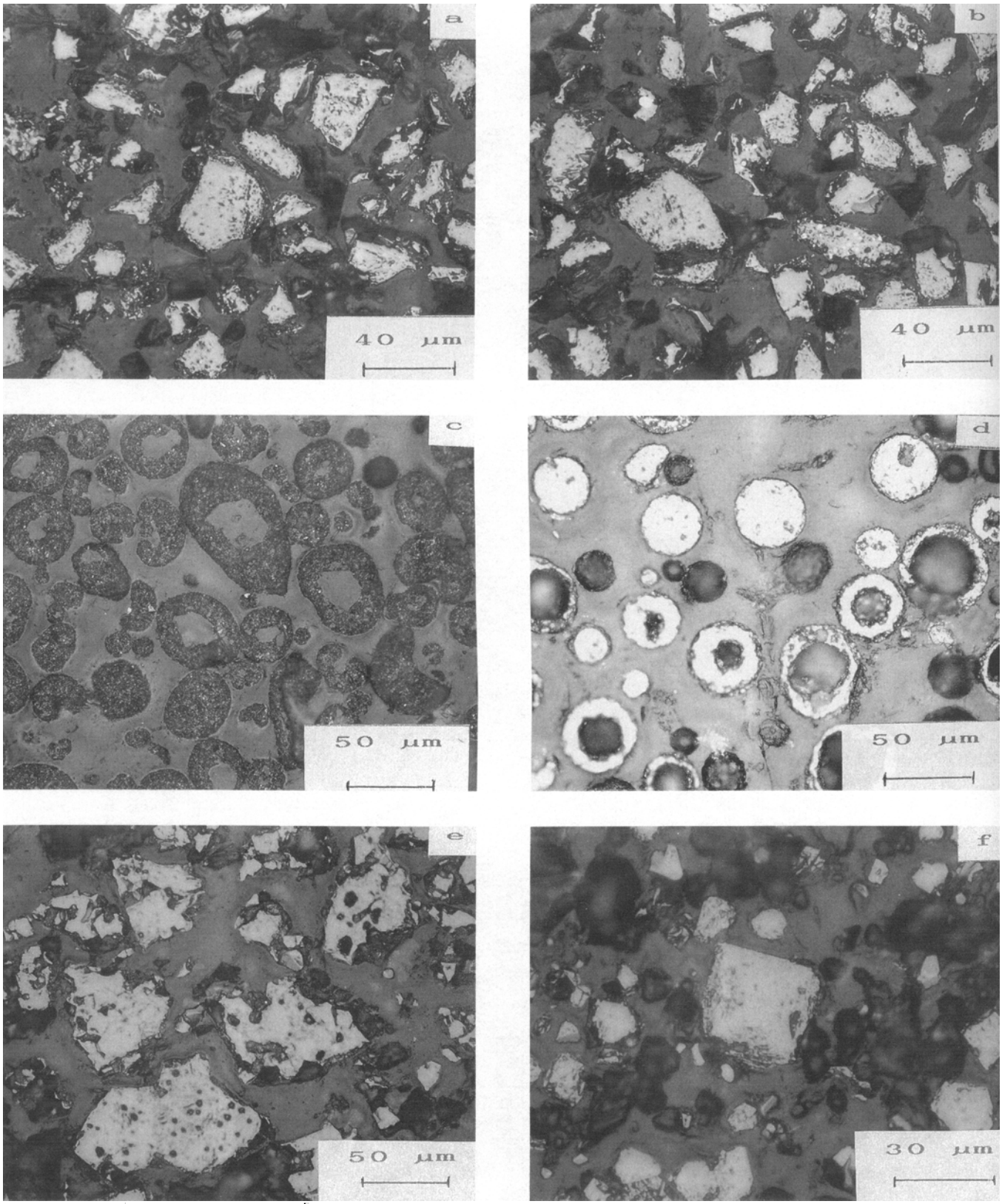

Fig. 3 Optical micrograph in bright field of internal morphology of chromium oxide powders produced using different techniques: (a) C technique; (b) SC technique (powder SC1), (c) A technique (powder A1); (d) A technique followed by arc plasma densification (powder A1D); (e) SC technique (powder SC2), (f) C technique

Some powders were submitted for microanalytical analysis with the use of the x-ray photoelectron spectroscopy (XPS) technique. The excitation source was magnesium Kα radiation having photon energy of 1253.6 eV. Other details of this analysis are described in Ref 7. Figure 4 shows Cr 2p spectra of the powders (FC, SC1, A1, and C) with an intense Cr $2p_{3/2}$ peak at a binding energy of 576.8 eV. This peak corresponds to Cr_2O_3, whereas the metallic chromium has a peak at 574.6 eV observed in samples of FC and SC1 powders. This confirms that the technique of fusing and sintering used in powder manufacture leads to the reduction of chromium oxide to the metallic chromium.

The quantitative XPS analysis (Table 3) indicates that all analyzed powders contain carbon. The presence of this element might be due to contamination during the XPS analysis or created by the organic binder (in A1 powder). The sodium discovered in SC1 and A1 powders arises from the use of the glass additive to the chromium oxide that contains not only silica but also sodium oxide. The Cr/O atomic ratio is the smallest in the agglomerated A1 powder. Chromium oxide pigment being agglomerated in this powder was submitted to very mild heat treatment (about 490 K at spray drying). Inversely, sintering and melting (the latter at a temperature as high as 2710 K) of chromium oxide that took part in the SC1 and FC powders manufacturing led to loss of oxygen in the treated material.

3. Thermal Spraying

The chromium oxide top coating could be sprayed by APS, VPS, and even high velocity oxygen fuel (HVOF) spraying (Ref 8). In the present study, the APS technique was applied to spray the particulate composite and top coatings.

3.1 *Optimization of the Coatings Deposition Process*

The optimum choice of APS parameters applied to deposit the top chromium oxide coating should result in the coating properties specified in Table 1. The particles of any chromium oxide powder used in the study are of different size and are porous inside.

The size of the particles determines their temperature and velocity at flight in the plasma flame generated by a torch working at given processing parameters (see Fig. 5) (Ref 9). Thus the powering of an APS torch at 25.2 kW allows full melting of particles smaller than 25 μm. An increase in electric power would result in a longer flame of higher temperature, which permits large particles to be melted. (From Ref 10, these phenomena occur as described up to a certain value of electric power, about 50 kW. Above this value, for a torch of 7 mm nozzle inside diameter, the velocity of jet increases, but its length and its temperature remain constant.) Porous particles, those of A1 and A2 powder, would require higher powers than the dense ones. The higher power would generate the hotter plasma necessary to overcome the effect of hampering the heat penetration by the pores inside the particles. The internal porosity has a negligible effect on the particle velocity, being determined mainly by their size. Thus large particles remain not only unmelted (or partly melted) but are also slower on the impact with the substrate. The particles decrease the quality of the sprayed coating because they lower the adhesion if deposited on the substrate and increase the porosity if deposited on the previously deposited coating. Thus they also lower the coating hardness and cohesion (see Table 1). These particles could be blown out of the flame by a compressed air barrier (Fig. 6). However, the blown particles should be immediately removed from the spray area by a strong local aspirator. Otherwise, the compressed air induces turbulence that can result in the agglomeration of the particles (coalescence) and their successive free fall on the sprayed coating. The result is that very large agglomerates become incorporated in the coating, which can decrease the quality of the following laser engraving.

The feeding of chromium oxide powder might be performed with the use of oxygen as a carrier gas. This gas, mixed with the flame at the torch outlet, renders the spray atmosphere less reducing and more favorable to spray oxides. However, as the viscosity of oxygen differs from that of the usual argon, a careful optimization of the carrier gas flow rate is necessary. Moreover, oxygen used as the carrier gas cools the plasma jet. The torch

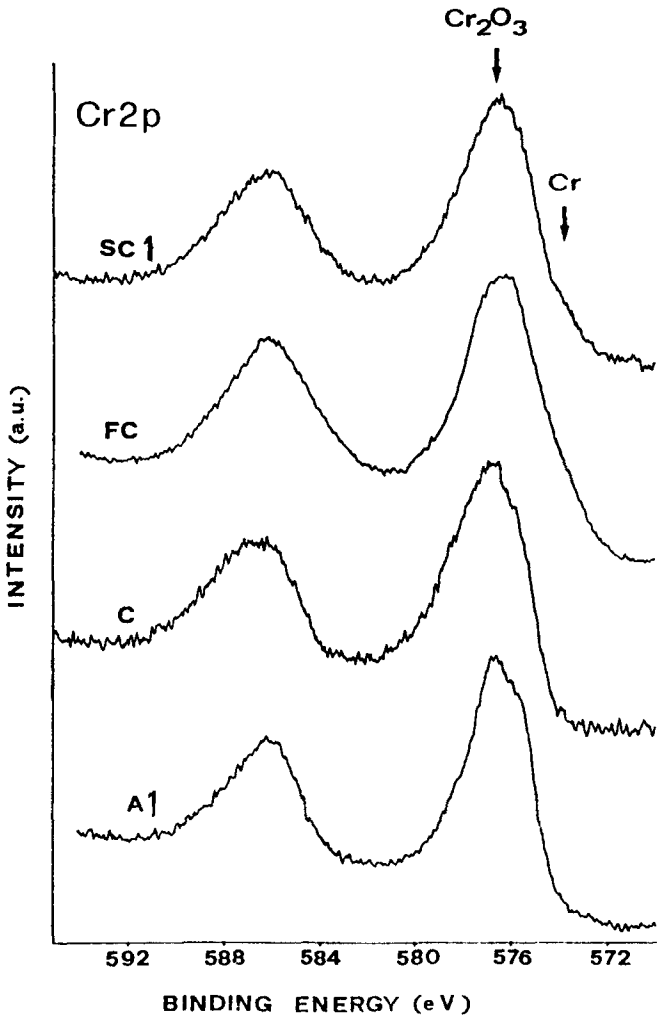

Fig. 4 XPS spectra of chromium oxide powders: SC1, FC, C, and A1 (Cr 2p photoelectron line)

must be supplied with higher electric power to compensate for this effect (Ref 7).

The reducing atmosphere in the plasma flame is mainly due to the presence of hydrogen as a secondary working gas. Hydrogen increases the enthalpy of the plasma jet and its thermal conductivity. Some torches under development enable spraying of chromium oxide using argon as a single working gas without using hydrogen (Ref 12).

In the case of engraving very deep cells (deeper than 50 μm), the top coating is submitted to the severe thermal shock at the laser treatment. Thus to avoid the cracking of the coating, spray the particulate composite coating, such as NiCr, with Cr_2O_3 between the bond and the top ones. This composite should possibly have a coefficient of thermal expansion (CTE) and an elastic modulus that is intermediate between those of the top and bond deposits. A possible way to achieve repetitive and precise manufacturing of such composites while plasma spraying consists of using two external powder injector ports that are at different distances from the torch nozzle. (Some other possible configurations of the powder injection ports are discussed in Ref 13.) The injector closer to the torch is used for the Cr_2O_3 powder.

Previous study (Ref 14) has shown that a total volume feed rate of the powder into the plasma flame (of F4 torch manufactured by Sulzer-Metco, Wohlen, Switzerland) of about 20 cm^3/min enables melting of most of the sprayed particles. (The particulate composite of Al_2O_3 with Al was tested in Ref 14.) The sum of the powder feed rates injected into plasma is equal to:

$$q_{Cr_2O_3} + q_{NiCr} = 20\ cm^3/min \quad \text{(Eq 1)}$$

where q stands for volume feed rate (q multiplied by the powder density gives the mass feed rate). The content of NiCr in the composite can be defined as:

$$\theta = \frac{q_{NiCr}}{q_{NiCr} + q_{Cr_2O_3}} \quad \text{(Eq 2)}$$

Although the parameter θ does not give the fraction of NiCr in the composite, it allows a direct link between its property (such as CTE) and the powder feeder operational parameter. The twin powder feeder used in the experiments was equipped with rotating plates. Thus the twin powder feeder supplies simultaneously NiCr and Cr_2O_3 powders during composite coating (Fig. 7) with a precisely calibrated feed rate.

The velocity of the torch over the roll influences the number of lamellae included in a layer deposited in one torch pass and the layer thickness. The AR production is less expensive if the total coating thickness is reached in as few torch passes over the

Table 4 Calculation of a roll rotation and torch traverse speeds for cylinders of different diameters for a spray torch linear velocity equal to 180 cm/s

AR diameters, mm	Rotation speed, 1/min	Traverse speed, mm/s
50	689	46
100	343	23
150	229	15
200	172	11
250	137	9
300	115	8

In the calculation it was assumed that during one rotation of cylinder, the torch moves a distance of 4 mm.

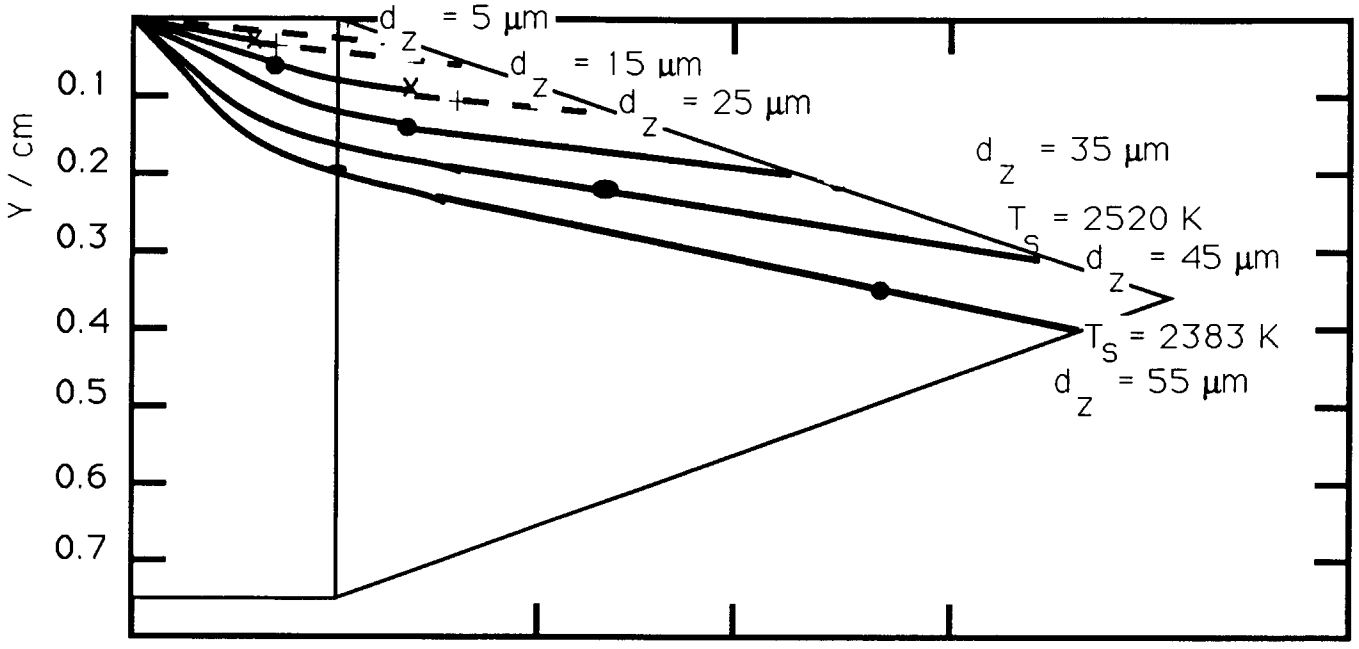

Fig. 5 Calculated trajectories and temperatures of the chromium oxide particles inside the plasma flame of the APS torch supplied with 42 Nl/min of argon, 5 Nl/min of hydrogen, and 25 2 kW of electric power (Ref 9). Symbols: d_Z is particle diameter, T_S is the temperature of the particle surface at the flame boundary; Lines: full line, particle solid or partly liquid; dashed line, particle fully molten; Points: closed circles, surface of particle reaches melting point; x, surface of particle reaches boiling point; +, particle becomes fully molten

roll as possible. In fact, Ref 15 mentions the possibility of a deposition of a 300 μm thick layer. However, quality of the chromia coatings deposited in this way would not be expected to be high because the temperature gradient across the layer could lead to the generation of thermal stresses and eventual cracking.

At present, it is assumed that the Cr_2O_3 coatings of reasonable quality could be obtained if a layer thickness ranges between 5 and 10 μm. Such coatings could be sprayed with a torch linear velocity of 180 cm/s. This velocity is composed of rotation and transverse speeds at spraying of AR (Table 4). It is necessary to make 30 to 60 passes of the torch over the roll to obtain the thickness of 300 μm. The number of passes can be reduced by a factor of 2 if two APS torches are used simultaneously to spray chromium oxide.

Finally, an application of the cryogenic cooling at the oxide coating (as it was shown in Ref 16 for zirconium oxide) could enable the deposition of thicker layers. Such cooling would lead to a decrease of the temperature gradient across the layer and could help in preserving the coating integrity.

Some parameters of deposition processes of the bond, particulate composite coatings, and top coatings discussed in the paper are collected in Table 5.

3.2 *Properties of Coatings*

3.2.1 Microstructure

The microstructure of the bond coat is discussed in Ref 17. The focus here is given on the top coats that are plasma sprayed with chromium oxide powder.

The FC powder resulted after spraying at a relatively low electric power (46 kW) in a very porous coating containing metallic inclusions (Fig. 8). The coating sprayed with low electric power and with an agglomerated A powder did not reveal such inclusions (Fig. 9).

An increase in electric power associated with higher working gas flow rates could result in better melting and higher velocity of sprayed particles. These particles on impact with the substrate

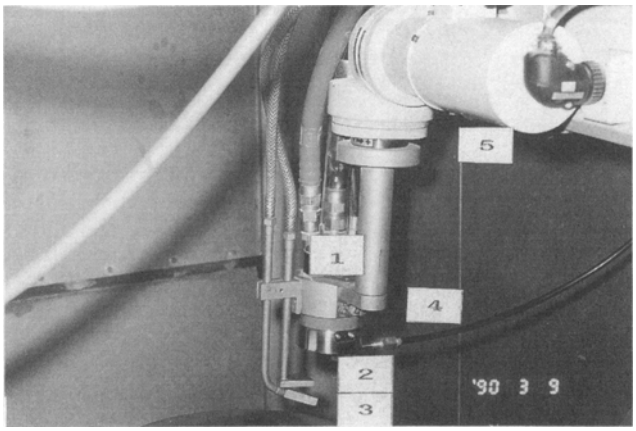

Fig. 6 APS torch with the compressed air barrier and cooling (Ref 11): 1, torch; 2, compressed air barrier; 3, compressed air cooling; 4, powder injector; 5, arm of an industrial robot

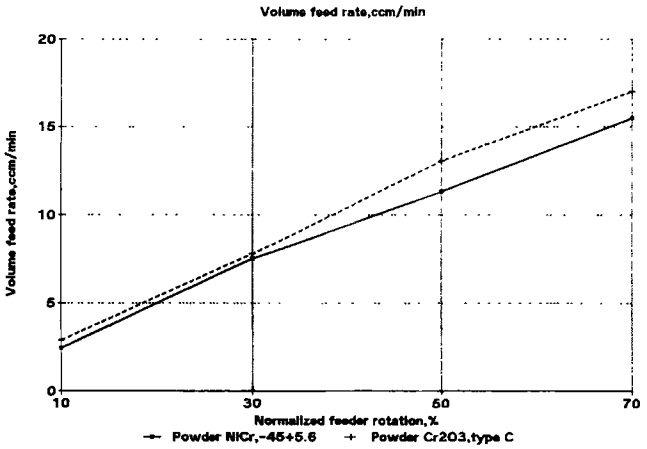

Fig. 7 Volume feed rate of NC powder (grain size –45 to 5.6 μm) and C powder versus normalized rotation speed of the twin powder feeder plate

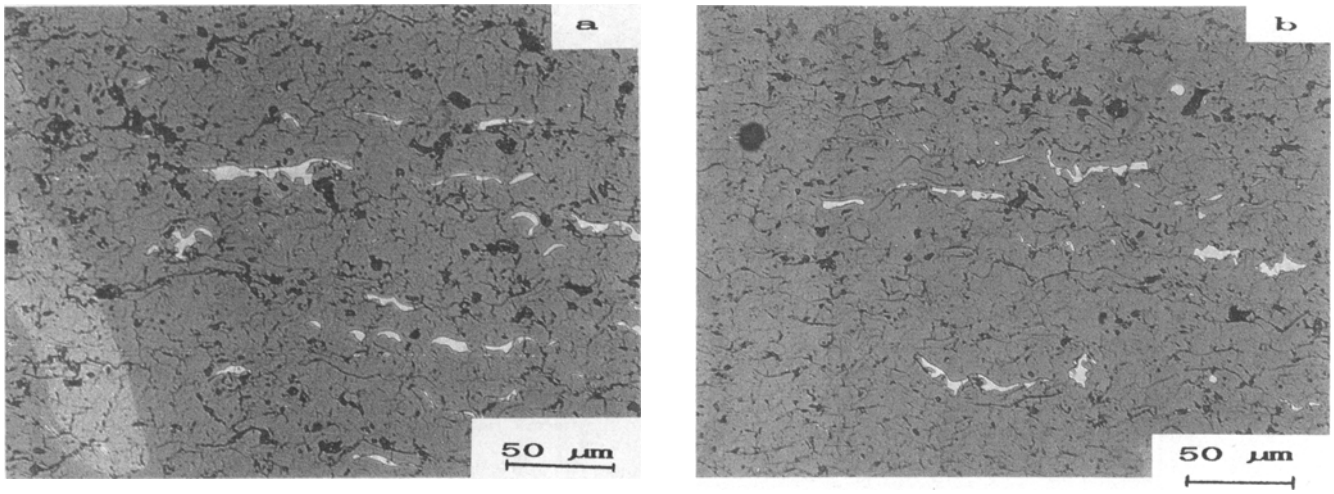

Fig. 8 Optical micrograph in bright field of the polished cross sections of the coating sprayed with FC powder and (a) 9th set of processing parameters and (b) 8th set of processing parameters (see Table 5)

give rise to a splat having a "flower" shape (Ref 18). In fact, that shape was observed for FC powder particles sprayed using high electric power (Fig. 10). Recent investigations concerning the impact of alumina and zirconia particles (Ref 19) reveal an influence of the substrate temperature on the shape of the splat. Similarly, the increase in electric power reduced the porosity of the sprayed coatings (Fig. 8b and 9b). The lamellae in the coatings sprayed with fine and "regular" size powders (that is powder with a d_{50} less or equal to 30 μm) show mainly a columnar structure (Fig. 11a). This indicates that the particles were melted at impact. The coatings sprayed using coarse powder (SC2) do not exhibit a lamellar structure (Fig. 11b). Thus the particles of this powder were not melted on impact. Moreover, the spherical pores visible inside the grains might result from dissolution of the gas during the flight of the molten particle. Rapid solidification of the melt entrapped the gas inside the lamellae. On the other hand, the impact of these coarse particles was not vigorous enough to deform the lamellae and to liberate the gas from the

Table 5 APS processing parameters of bond coating, top coatings, and particulate composite coating considered for AR production

Parameter set	Coating type	APS torch	Electric power, kW	Working gases flow rate, NL/min	Carrier gas flow rate, NL/min	Spray distance, cm	Compressed air barrier
1	Top	TS6	53	50(Ar), 14(H_2)	6 (O_2)	10	Yes
2	Top	TS6	53	50(Ar), 14(H_2)	6(Ar)	10	Yes
3	Top	TS6	42	50(Ar), 14(H_2)	6(O_2)	10	Yes
4	Top	TS6	53	50(Ar), 14(H_2)	6(O_2)	7	Yes
5	Top	TS6	45	50(Ar), 14(H_2)	6(O_2)	10	Yes
6	Top	TS6	49	50(Ar), 14(H_2)	6(O_2)	10	Yes
7	Bond	F4	28	35(Ar), 14(H_2)	6(Ar)	9	Yes
8	Composite and top	F4	50	60(Ar), 12(H_2)	7(O_2)	10	Yes
9	Top	F4	46	45(Ar), 13(H_2)	5(Ar)	10	Yes
10	Top	Custom built	34	70(Ar), 20(H_2)	5(Ar)	70	Yes
11	Top	PN-120	28	42(Ar), 11(H_2)	5(Ar)	100	No

APS torch TS6 is from SNMI, Avignon, France. F4 is from Sulzer-Metco, Wohlen, Switzerland. Custom built APS torch is from Limoges, France. PN-120 is from Otwock, Poland

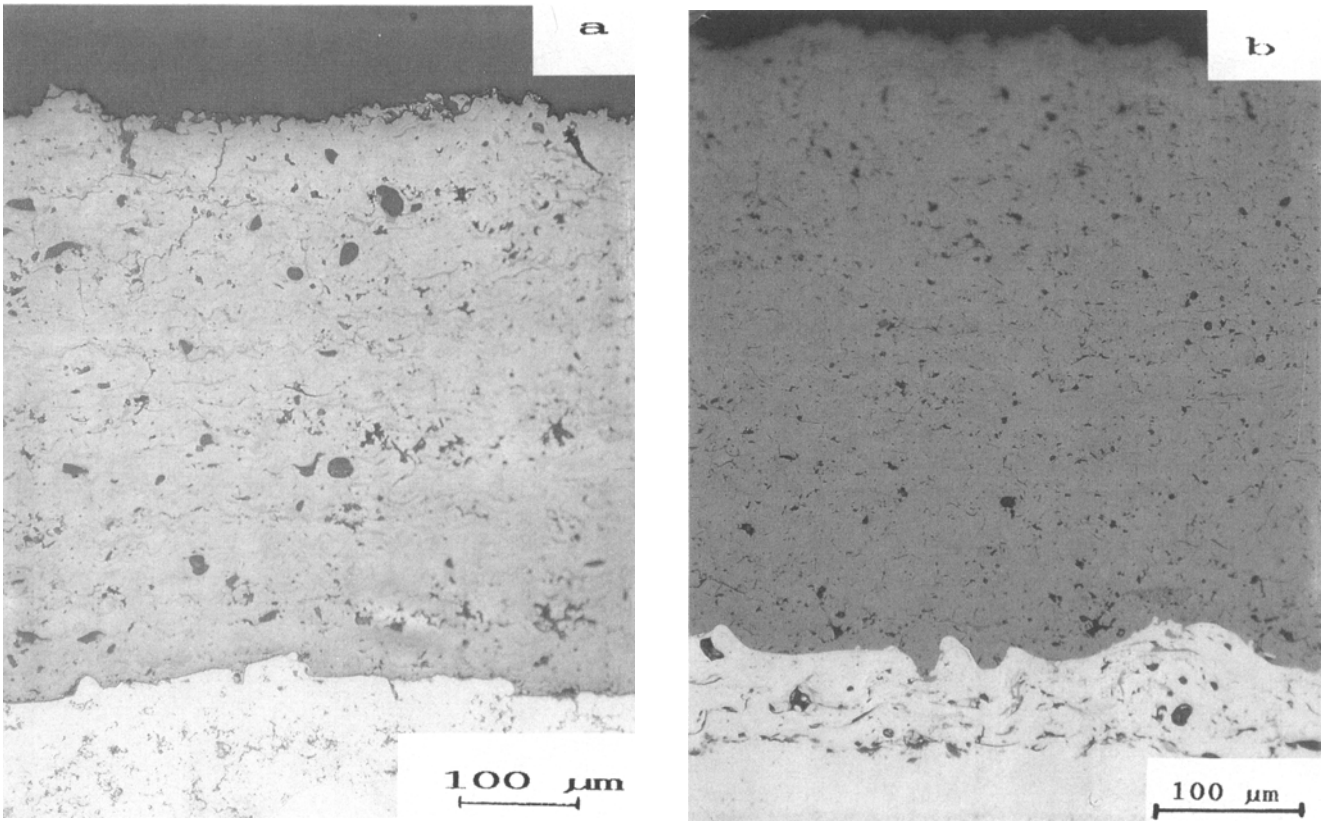

Fig. 9 Optical micrograph in bright field of the polished cross sections of the coating sprayed with Al powder and (a) 11th set of processing parameters and (b) 1st set of processing parameters (see Table 5)

pores. Better deformation of lamellae would be achieved by application of considerably higher electric power (if the APS installation enables it) or even with the high energy plasma spraying (HEPS) technique (see Ref 20).

Table 6 shows the XRD analysis of the powders and the coatings. SiO_2 is present in A1, SC1, and SC2 powders as quartz and crystobalite but is not present in their corresponding coatings. Most probably, SiO_2 has partially evaporated from the particles during flight in the plasma jet. The variation in processing parameters, such as the carrier gas, the spray distance, and the electric power used to spray A1 powder, does not influence the crystal phase content. The eskolaite is the only phase identified in most of the sprayed coatings. An exception is the coating sprayed with FC powder that contains a small quantity of the Cr_3O_4 oxide. In coatings sprayed using an earlier batch of the same FC powder (bought from the same manufacturer a few years earlier), the coatings sprayed using similar parameters showed the presence of CrO and of metallic chromium. This indicates an improvement in the quality of FC powder produced recently. Finally, the powders commercially available produce coatings of reasonably similar phase content.

An origin of one of the inhomogeneities in the chromium oxide coatings is the oxygen loss at spraying. Oxygen loss has been reported in APS coatings of $YBa_2Cu_3O_x$ high critical temperature (T_c) superconductor (Ref 21) or $Ni_{0.35}Zn_{0.65}Fe_2O_4$ ferrite (Ref 22). The postspraying treatment at high temperatures (800 K or higher) in oxygen or air restored the oxygen content. Unfortunately, this procedure cannot be adopted for the AR because annealing of the rolls would probably result in spallation of the chromium oxide coating. Thus a correct choice of powder and optimization of deposition processing parameters must be performed.

The XPS technique was applied previously (Ref 23 and 24) to determine the oxygen losses in zirconium oxide coating. This technique enabled detection of carbon in the tested samples (Table 7). The presence of this element arises from contamination from the ambient environment during the analysis (Ref 7). The comparison of the XPS data concerning the atomic ratios Cr/O and Cr/Si obtained for powders (Table 3) and the corresponding coatings (Table 7) show the loss of silicon and oxygen (except for the coatings sprayed using FC powder). The silicon could be lost by the selective evaporation of silica as confirmed by XRD analysis (Table 6). The samples sprayed using A1 powder exhibit the lowest Cr/O ratio and, thus, the lowest loss of oxygen for this coating. This powder was therefore selected for further investigations. The XPS analysis of samples sprayed using different spraying parameters (Table 8) shows that the first set of parameters (see Table 5) produces coatings with the lowest oxygen loss. The application of argon as a carrier gas (second set of parameters) favors oxygen loss. On the other hand, the coating with a short spray distance (7 cm; see fourth set of parameters in Table 5) shows low silicon loss. Thus silica evaporation occurs at distances greater than 7 cm from the torch. Finally, the lowering of the electric power supplied to the torch (down to 42 kW as in the third set of parameters) does not lead to lower losses of oxygen or silicon.

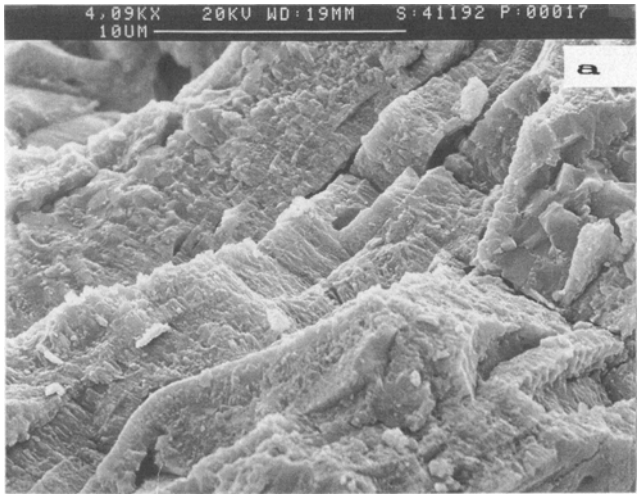

Fig. 10 SEM (secondary electrons) micrograph of a splat formed after impact of FC powder particle sprayed with 8th set of processing parameters (see Table 5)

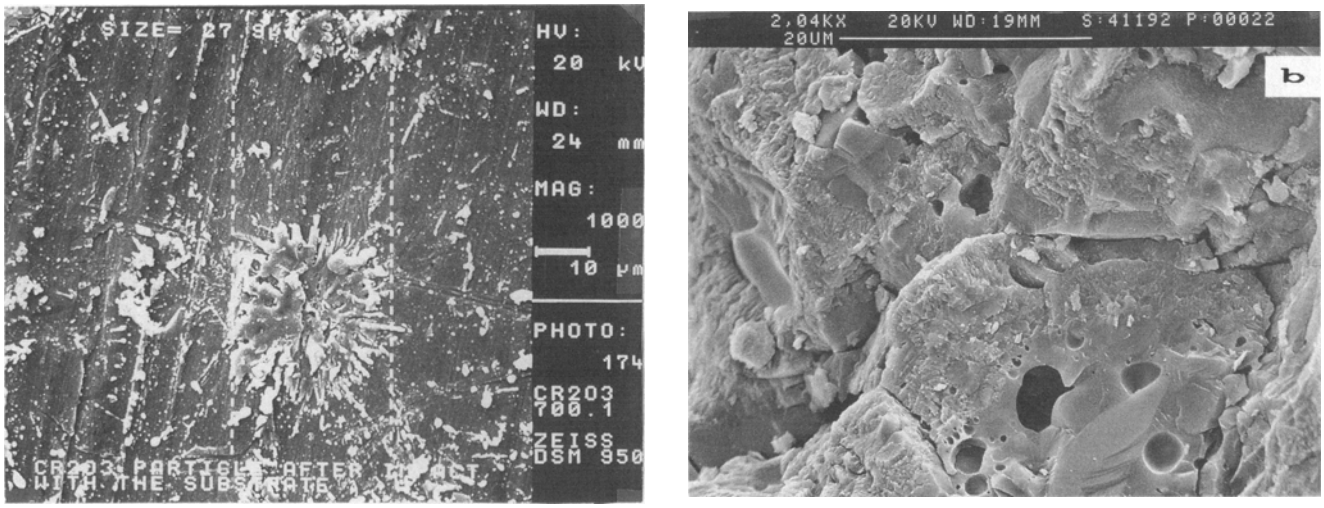

Fig. 11 SEM (secondary electrons) micrograph of the fractured sections of the coating sprayed using (a) A1 powder with 2nd set of processing parameters and (b) SC2 powder with 5th set of processing parameters (see Table 5)

Table 6 XRD phase analysis of the powders manufactured using different techniques and the corresponding plasma-sprayed coatings

Powder type	Cr_2O_3, eskolaite(a)	SiO_2, quartz(b)	SiO_2, crystobalite(c)	Coating sprayed using parameter set shown in Table 5	Cr_2O_3, eskolaite	Cr_3O_4(d)
FC	Major			5	Major	Minor
A1	Major	2 Minor	1 Minor	1	Major	
				2	Major	
				3	Major	
				4	Major	
SC1	Major	2 Minor	1 Minor	2	Major	
SC2	Major	1 Minor	2 Minor	4	Major	
C	Major			5	Major	

Note: In the multiphase powders or coatings, the phases are ordered by decreasing content: major, 1 minor, 2 minor, etc (a) Identified using ASTM file 6-504. (b) Identified using ASTM file 33-1161. (c) Identified using ASTM file 11-695 (d) Identified using ASTM file 12-559.

Table 7 Quantitative XPS analyses of chromium oxide coatings

Powder type	Set of parameters	Element concentration, at.%					Atomic ratio	
		Cr	O	C	Si	Na	Cr/Si	Cr/O
FC	5	19.1	46.9	34.0	...	...	...	0.41
SC1	5	26.8	51.6	19.4	2.2	...	12.2	0.52
A1	1	17.2	55.6	21.7	2.9	2.6	5.9	0.31

See parameter set in Table 5.

Table 8 Quantitative XPS analysis of coatings sprayed with an agglomerated A1 powder

Set of parameters	Element concentration, at.%					Atomic ratio	
	Cr	O	C	Si	Na	Cr/Si	Cr/O
1	17.2	55.6	21.7	2.9	2.6	5.9	0.31
2	22.1	50.7	18.3	3.9	5.0	5.7	0.43
3	23.7	50.8	15.7	2.4	7.4	9.9	0.47
4	21.2	54.0	13.3	5.8	5.7	3.6	0.39

See parameter set in Table 5.

The presence of sodium in the coatings was attributed (Ref 7) to the formation of compound Na_2CrO_4. This compound is a product of the reaction between Na_2O (included in silica glass used to agglomerate the A1 powder) and Cr_2O_3. The reaction could start in the particle splat upon cooling at a temperature of 1100 K.

3.2.2 Physical Properties of Coatings

The open porosity of the chromium oxide coatings was measured by the Archimedean technique (samples sprayed using APS torch F4) and with the commercially available mercury intrusion porosimeter (MIP) (model 2000 of Carlo Erba Milan, Italy). Samples were sprayed using APS torch TS6. Results of the porosity investigations (Fig. 12) reveal very low open porosity (about 2.5%) of the coating sprayed using the C powder. The open porosity (by MIP) of the samples sprayed using FC powder and the TS6 torch is also very low. This is not confirmed by measurements (by Archimedean method) of samples obtained using this powder and the F4 torch. The discrepancy might come from different parameters of the coating, different porosity measurement methods, or different batches of FC powder used. The porosity of the A1 agglomerated powder coating is about 6.5% and is similar to the porosity of SC1 powder coating (about 6.4%).

The CTE of the particulate composites of NiCr and C type chromium oxide sprayed with the F4 torch was measured (Fig. 13) as a function of the NiCr content in the composite. Measurements were made using a Netsch 402E dilatometer in the temperature range of 300 to 470 K at the heating rate of 3 K/min. Composites were characterized by the θ parameter (see Eq 2). Coatings with θ parameter of 0 (pure chromium oxide), 0.3, 0.5, 0.7, and 1 (pure nickel chromium coating) were tested. The desired composite, to be applied between the bond and top coatings, should have the CTE intermediate between that of these coatings, for example

$$\mathrm{CTE\,(composite)} = \frac{\mathrm{CTE}(Cr_2O_3) + \mathrm{CTE(NiCr)}}{2} \qquad \text{(Eq 3)}$$

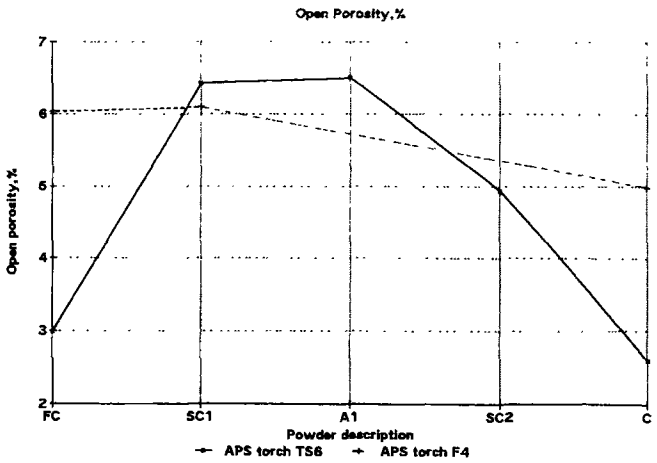

Fig. 12 Open porosity of the coatings sprayed using FC, SC1, and SC2 powders with 5th processing parameters (solid line), A1 powder and 1st set of processing parameters (dashed line), C powder and 6th set of processing parameters (dashed line), FC and C powders and 8th set of processing parameters (dashed line) (see Table 5). Experimental points are joined together for clarity.

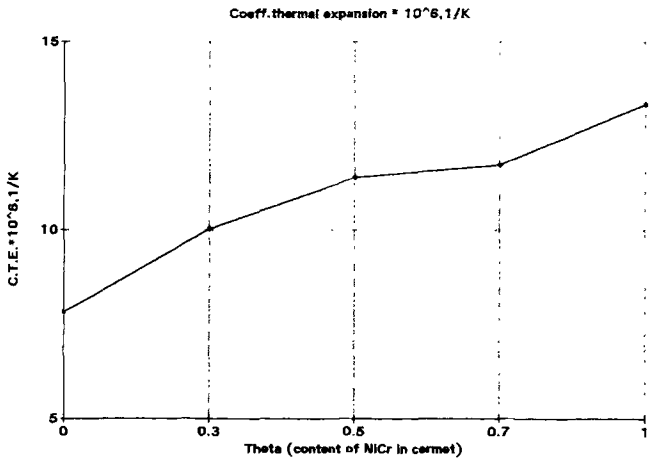

Fig. 13 Coefficient of thermal expansion (CTE) of the particulate composite coatings sprayed using NC and C powders with 8th set of processing parameters versus content of NiCr in the composite (see Table 5). Experimental points are joined together for clarity.

Figure 13 indicates that this composite is characterized by the parameter $\theta = 0.4$. Subsequently, Eq 2 enables the volume feed rate of NiCr powder to be calculated as:

$$q_{NiCr} = \theta(q_{NiCr} + q_{Cr_2O_3}) = 0.4 \times 20 = 8\ cm^3/min \qquad (Eq\ 4)$$

The volume feed rate of chromium oxide C type powder is equal to 12 cm^3/min. Finally, Fig. 7 shows the operational settings of the twin powder feeder, which are 35% for NiCr powder and 49% for the Cr_2O_3 type C powder.

The method described here was previously applied to optimize the CTE of Al-Al_2O_3 composites (Ref 14) and can be adopted easily to other types of powder feeders.

CTEs of the chromia coatings sprayed using different powders do not differ significantly (Fig. 14). The coefficients measured in the temperature range of 300 to 473 K are slightly greater than those measured in the temperature range of 300 to 373 K.

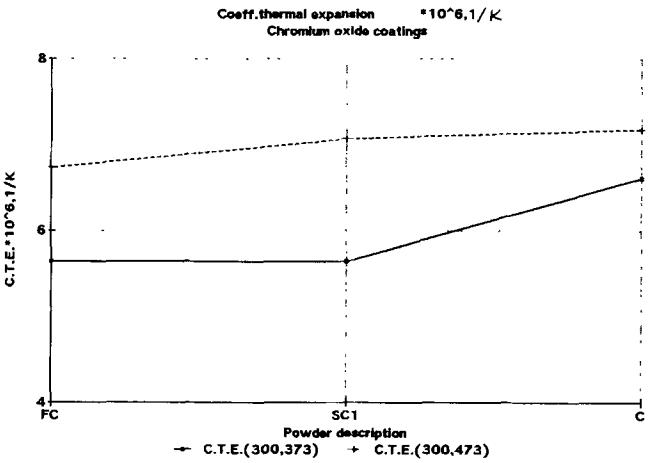

Fig. 14 Coefficient of thermal expansion (CTE) measured at temperatures from 300 to 373 K (solid line) and 300 to 473 K (dashed line) of the coatings sprayed using FC, SC1, and C powders with 8th set of processing parameters (see Table 5). Experimental points are joined together for clarity.

3.2.3 Mechanical Properties of the Coatings

The microhardness of chromia coatings was measured on the metallographically polished longitudinal cross sections (the sections are perpendicular to the coating surface). The Shimadzu tester was used in this study under load times of 15 s.

The Vickers microhardness under a load of 3 N (HV_3) of the coatings sprayed with different powders (Fig. 15) is for all sprayed coatings greater than 1000 and that meet the criteria specified in Table 1. The coatings sprayed using agglomerated A1 and crystalline C powders have the highest values of microhardnesses (about $HV_3 = 1250$). The literature on sprayed chromia reports values as high as $HV_2 = 1890$ (Ref 25) and $HV_2 = 1990$ (Ref 26) for coatings deposited with the HEPS technique.

The choice of load while testing the microhardness strongly influences the measured values. The low load values show the microhardness of the individual lamellae, while the high load measurements describe the microhardness of the coating that depends on the strength of interlamellar contacts and on the porosity (Ref 3). The individual lamellae are always harder than the bulk coating (see Fig. 16), and the low load microhardness values as high as $HV_{0.5} = 1700$ are not surprising (coatings sprayed using A1 powder). On the other hand, an exceptionally great value of high load microhardness of $HV_{20} = 1000$ was found for chromium oxide sprayed with powder C. This value suggests good contact between the lamellae within the coatings of lowest open porosity of 2% (see Fig. 12).

The agglomerated A1 powder contains a lot of internal porosity (see Fig. 3), which might also exist in the sprayed coatings. Subsequently, the microhardness is expected to be rather low. However, an optimum choice of the spraying parameters (especially in altering the electric power) enabled a HV_3 microhardness of A1 powder coatings as great as that of the powder C to be obtained.

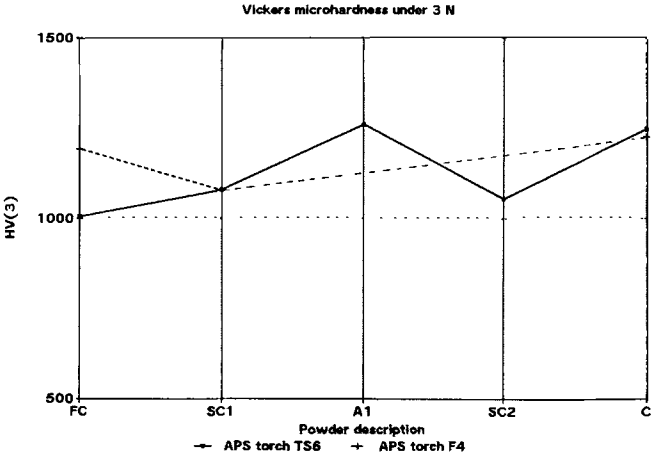

Fig. 15 Vickers microhardness under load 3 N of the coatings sprayed using FC, SC1, and SC2 powders with 5th set of processing parameters (solid line), C powder with 6th set of processing parameters (solid line), A1 powder with 2nd set of processing parameters (solid line), FC, SC1, and C powders with 8th set of processing parameters (dashed line) (see Table 5). Experimental points are joined together for clarity.

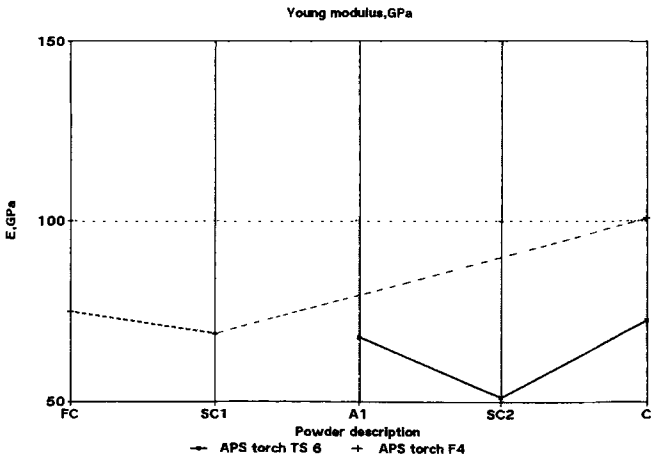

Fig. 17 Young modulus of the coating sprayed using SC2 and C powders with 5th set of processing parameters (solid line), A1 powder with 2nd set of processing parameters (solid line), FC, SC1, and C powders with 8th set of processing parameters (dashed line) (see Table 5) Experimental points are joined together for clarity.

The bond strength of chromia top coating sprayed with powder type C and the APS torch F4 was tested using ASTM standard C 633-69 (standard test method for adhesive and cohesive strength of flame sprayed coatings, 21 March 1969).The mean value of the bond strength for five coated mild steel samples was about 20.9 MPa. This value is similar to that obtained in Ref 27 (25.4 MPa). On the other hand, a careful optimization of the initial temperature prior to plasma spraying of the Cr_2O_3 powder onto mild steel substrates enabled Funk et al. (Ref 28) to achieve bond strength as high as 61 MPa. The initial temperature of 513 K applied by these authors is not practical for AR of large dimensions. Subsequently, an increase in the bond strength has to be achieved by an application of the well-adhering bond coating.

The elastic modulus of the free standing coatings was determined using an ultrasonic technique with a device by Grin-

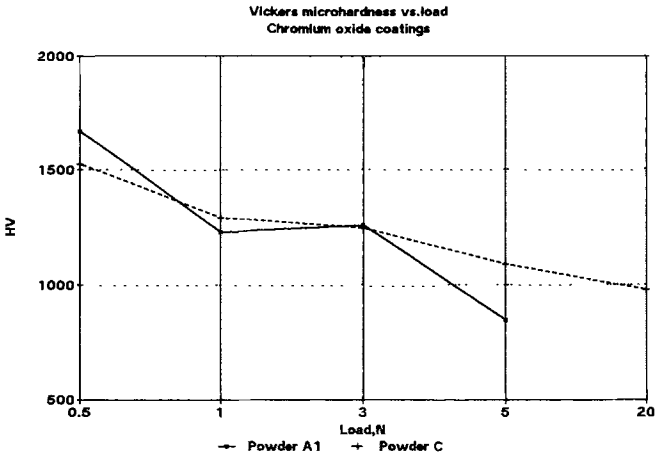

Fig. 16 Vickers microhardness versus load of the coating sprayed using A1 powder with 2nd set of processing parameters (solid line) and C powder with 6th set of processing parameters (dashed line) (see Table 5). Experimental points are joined together for clarity.

dosonic of Elektronika Ltd., Leuven, Belgium. Results of the determinations shown in Fig. 17 indicate that the modulus of sprayed coatings is in the range of 15 to 32% of the value for the sintered chromium oxide (E = 314 GPa for the sintered chromium oxide, from Ref 29). The coating sprayed with the C powder and F4 torch has the greatest elastic modulus, E, of 100 GPa. This value is less than that of 138 GPa found by Richard et al. (Ref 29), but it is quite smaller than 180 GPa determined using the ultrasonic method in Ref 30.

4. Postspraying Treatment

4.1 *Finishing*

The surface of the coating on the AR under service conditions must remain in close contact with respect to the doctor blade. Therefore, the local changes of contact (due to the coating roughness) and systematic ones (due to poor concentricity of the roll) have to be reduced. This might be achieved by grinding to obtain a specified concentricity of less than 0.02 mm followed by polishing to obtain a specified roughness.

The R_a coefficient, which is frequently used to describe roughness, is less useful in AR technology. The R_a describes a mean value of the roughness without taking into account the highest or deepest points along the analyzed line. More useful is the R_z coefficient, which is defined as:

$$R_z = \frac{1}{5}\left(\sum_{i=1}^{5} Y_{ip} + \sum_{i=1}^{5} Y_{iv}\right) \quad \text{(Eq 5)}$$

where Y means absolute height of one of the five highest peaks (index p) and absolute depth of one of five deepest valleys (index v) along the analyzed line. This parameter has to be measured in a few places along the coating surface.

Diamond wheels with a resin matrix are typically used to grind chromium oxide sprayed coatings. The grinding can be made in two stages, starting with a diamond size of about 100

μm and followed by grinding with another wheel of diamond size about 50 μm.

The total thickness of the coating ground off is about 100 μm. The grinding parameters, such as rotation speed of a diamond wheel, rotation speed of the roll, and depth of the grinding depend on the dimensions and weight of the roll.

The desired roughness can be achieved by polishing. These diamond wheels have grain sizes ranging from 30 to 7 μm.

Sometimes after polishing, there are grinding artifacts resulting from machine vibration. In such situations, these features can be removed by lapping using very fine diamond or alumina pigment (submicron size) in an oil or grease mixture.

The final roughness of the finished coating is difficult to specify. In practice, one often applies roughnesses lower than R_z = 5 μm. Obviously, smooth surfaces are necessary if the following engraving should give shallow cells. This is to ensure that peaks and valleys resulting from roughness are significantly smaller than the cells. On the other hand, a large part of laser light energy is reflected when the engraved surface is smooth. This effect was discovered for a roll of a diameter 54 mm and length 160 mm, coated with C powder. This roll was finished to obtain three different roughnesses and then treated with the laser. Laser parameters were kept constant. The desired line density was LD = 140 1/cm, and the desired cell depth was about 15 μm. The resulting depths of the cells (see Table 9) were clearly deeper for the rougher surfaces. This result indicates that when engraving such surfaces, a great part of the laser energy is absorbed and used to evaporate the coating material.

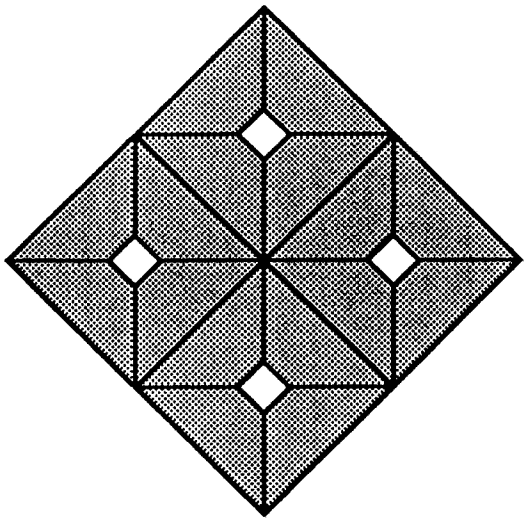

Fig. 18 Four truncated pyramid cells in a mechanically engraved and chrome plated AR

Table 9 Cell depth of chromium oxide plasma-sprayed coatings

Roughness	R_z, μm	Cell depth, μm
Smooth	1.0-1.3	16.7
Average	1.8-2.2	17.9
Rough	3.4-4.0	18.1

4.2 *Engraving Process*

The most important function of the anilox roll is to transfer the precise quantity of ink from the ink container to the printing roll (see Fig. 1). The volume of the ink transfer, expressed in cm^3 (of ink)/m^2 (of the roll), is the parameter describing this function. This volume depends on properties of ink, such as viscosity, its base (water or oil) and the content of solid (Ref 31); ability of adsorption of the ink by the anilox roll surface, described by the wetting angle; and morphology of cell on the anilox roll, for example their shape (pyramid, truncated pyramid, etc.), depth, and their density (described by the number of lines containing cells in 1 cm, that is, line density).

As far as the line density (LD) is concerned, the fine pattern aniloxes (great line densities) have an advantage of enabling the precise determination of ink volume (Ref 32) and of giving better resolution of a printed pattern (Ref 33). Finally, the AR has to be engraved in such a fashion that allows the application of different inks. This possibility depends, in part, on the maintenance of engraved rolls (Ref 33), that is preventing ink from drying in the cells and cleaning out the ink from the AR after the printing run with an appropriate solvent.

On the other hand, the AR must be engraved in such a way that does not allow ink accumulation (without open pores or cracks).

4.2.1 Electronic Engraving Process

The AR can be produced by an electronic engraving procedure in which every cell is indented on a roll surface by a diamond. For large pattern aniloxes (up to 80 lines/cm; from Ref 31), the cells are engraved directly in the rolls. The finer pattern ARs are galvanically coated with a copper coating prior to engraving. The diamond engraving is followed by a chrome plating (sometimes two subsequent chrome platings are used to achieve a thicker deposit). The resulting chromium coating is 10 to 20 μm thick. The cells in these ARs are mainly pyramids or truncated pyramids and have a 45° orientation (see Fig. 18) with regard to the roll axis. The ink transfer volume in mechanically engraved rolls can be analytically calculated (as a sum of the pyramid volumes included in 1 m^2 of the roll). The line density of the rolls in the present market is up to 220 lines/cm, and the chrome-plated rolls have a lifetime in service of several months.

4.2.2 Laser Engraving Process

Chromium oxide has a lower wetting angle than galvanic chromium, especially for water-based inks. The plasma sprayed and finished Cr_2O_3 coatings are engraved with the laser working in a pulsing mode (Fig. 19). The roll is fixed in the engraving unit (1) in a way that ensures the roll concentricity while engraving. The roll surface speed and laser beam linear movement (starting from position 4 at the beginning of engraving to position 3 by its end) are controlled by a control unit (7) and a microcomputer (6). This unit enables the electronic regulation of the laser pulse length and its amplitude (monitored with a calorimeter, 5). The high-power CO_2 laser is used in most engraving installations. The composition of the lasing medium determines the pulse shape. For example, the fraction of nitrogen in the las-

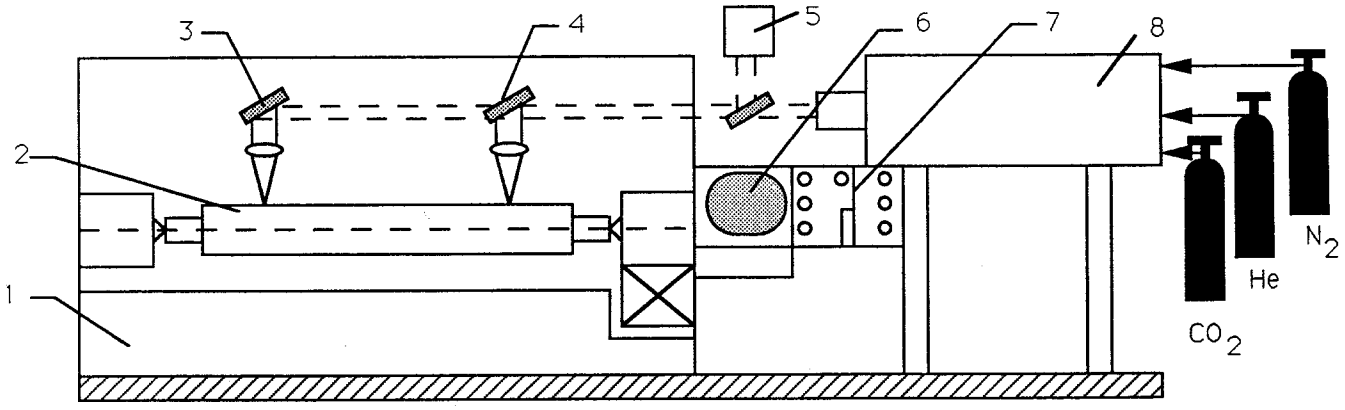

Fig. 19 Sketch of a laser engraver: 1, engraving unit; 2, anilox roll; 3, end of engraving; 4, beginning of engraving; 5, calorimeter; 6, microcomputer; 7, laser and engraving control unit; 8, high power CO_2 laser

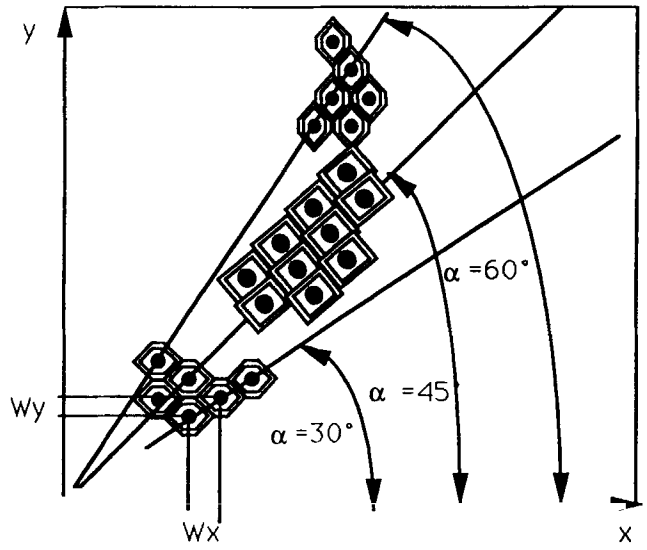

Fig. 20 Shape of the cells resulting from engraving at 30°, 45°, and 60°

ing mixture $CO_2 + N_2 + He$ should be kept low to reduce the pulse tail. This is of special importance while engraving a pattern with a high density of lines. An important engraving parameter, that is, the distance between the final laser lens and the engraved surface, has to be set manually prior to processing.

4.2.3 Optimization of the Laser Engraving Process

The ink transfer of laser engraved ceramic anilox rolls is slightly greater than that of a chrome-plated roll (of the same line density and cell depth) due to better wettability of ceramics and due to the form of cells. In fact, some manufacturers estimate that the ceramic rolls transfer 15% more ink than equivalent mechanically engraved ones (Ref 32).

The patterns engraved on the anilox rolls can be roughly divided into large (large pattern anilox) and fine (fine pattern anilox) arrays.

One cell in the large pattern aniloxes is engraved in many passes of a laser beam on the roll surface. Conversely, a cell in a fine pattern anilox is engraved in one pass of the laser beam, and usually one cell is engraved by one laser pulse. The fine pattern aniloxes are discussed further.

The principal parameters influencing the volume of the ink transfer and the quality of printing of ceramic AR are line density, angle of engraving, cell depth, and cell quality. Moreover, the time of engraving is an important factor that influences the cost of AR production.

The LD is usually measured with a microscope fixed on the roll surface. The microscope has an objective that can move with a calibrated precision in the x-y-z directions (x-axis follows the roll axis, y-axis is perpendicular to the roll axis, and z-axis is perpendicular to the roll surface). The measure consists of setting the focus on the center of one cell and moving the objective to the center of the next one in x or y directions. For example, the displacement in the x-direction, W_x, in micrometers and angle of engraving α (see Fig. 20) enables the line density (LD in 1/cm) to be calculated from the formula:

$$LD = \frac{10{,}000 \sin\alpha}{W_x} \qquad \text{(Eq 6)}$$

Modern laser engravers enable line densities up to about 400 lines/cm to be achieved. A proposal was made (Ref 34) to standardize the line densities to the values of 60, 80, 120, 195, etc. lines/cm. Variation of the volume of the ink transfer would result from the cell depth variation.

The angle of engraving results from the superposition of the movements of the roll rotation and the laser beam linear displacement. This angle can be set by software of the control unit prior to an engraving run. Again, the laser engraver enables optional engraving angles, but the standard ones, shown in Fig. 20, are 30° (cells look like a honeycomb with the longer axis in x direction), 45° (cells look like squares), and 60° (cells look like a honeycomb with the longer axis in y direction).

The actual engraving angle on a roll angle can be determined with a microscope by measuring the W_x and W_y displacements (see Fig. 20). The angle is also related to a pitch (μm), that is a displacement of a laser beam during one rotation of a roll, to a drop (%) describing the shift of the neighboring engraved lines and to a line density (LD in 1/cm) by the relationship:

$$\alpha = \arctan\left(\frac{\text{drop} \times 100}{\text{LD} \times \text{pitch}}\right) \quad \text{(Eq 7)}$$

The cell depth results from laser pulse power amplitude and length. The pulse length in the CO_2 laser depends on the lasing gases mixture composition (Ref 35). If a high frequency of laser pulses is required, then it becomes necessary to reduce the decay time of the pulse tail. Otherwise, the pulses overlap each other, and the engraved cells are joined together. In practice, reduction of the nitrogen fraction in the lasing gas mixture is a simple way to reduce the decay time of the pulse tail.

The cell depth in an engraved roll is usually determined by microscopy. Obviously, the top coating thickness must be greater than the cell depth. In practice, the 100 μm distance between the bottom part of the cells and the top of the bond coating would ensure the protection at the roll service of the bond coating against any undesirable contact with the ink.

The wall of the cells should resist the pressure of the doctor blade at printing. The wall thickness results from the length of the laser beam pulse and its surface speed.

The cell depth must be equal over all of the roll surface. The uneven depths result from differences in the pulse energy absorbed by the coating. First, the beam of a misaligned laser has different power density on the beginning of the roll than that on its end (see Fig. 19). Second, the absorption of the beam energy can vary with respect to the coating local microstructure. In particular, the presence of many unmelted grains in the engraved zone of the coating leads to sharp variations in the absorbed beam power. The resulting engraving would show (see section 4.2.4) areas of totally different depths.

As far as the engraving quality is concerned, the cells must not be fractured (see section 4.2.4) to avoid the ink accumulation. A top coating without fracture is a prerequisite to this achievement. As far as generation of fractures at engraving is concerned, it results from the superposition of many parameters, such as beam surface velocity, pulse length, and amplitude. Postengraving impregnation with an epoxy resin could be a practical way to reduce the effect of the fracture generation.

The cell shape is also important. First, the overflow (Fig. 21) is an effect that is difficult to avoid but must be reduced. This effect results from ceramics that become molten upon action of a laser pulse and, after being blown out of the cell, remain deposited on the surface of the cell walls.

The force that makes molten material emerge from a cell results from the expansion of gases inside the coating pores. Thus a decrease in coating porosity is favorable to reducing the overflow. Similarly, negligible overflow effect could be reached by such a choice of laser parameters that minimizes the thickness of liquid chromia during the action of laser pulse.

The cell shape should be Gaussian to facilitate comparison with the pyramid-like cells on the mechanically engraved rolls and to facilitate the calculation of the ink transfer volume. This shape could be achieved by setting the distance between the last lens and the roll surface greater than or equal to the lens focus (see Fig. 22).

Moreover, the Gaussian shape of cells is readily achieved by engraving with a laser beam having a Gaussian profile. This is achieved by a laser working in the TEM_{00} mode. (Transverse electromagnetics mode, TEM, describes the shape of the electromagnetic wave in the laser cavity. The index 00 refers to a fundamental mode of highest symmetry. The laser working in a mode TEM_{00} has a beam with a Gaussian distribution of energy.) Finally, the cell shape and an increase in the engraving speed (up to 10,000 cells/s) is equivalent to a reduction of the engraving time that could be achieved by using systems that apply multiple pulses in one cell (Ref 36).

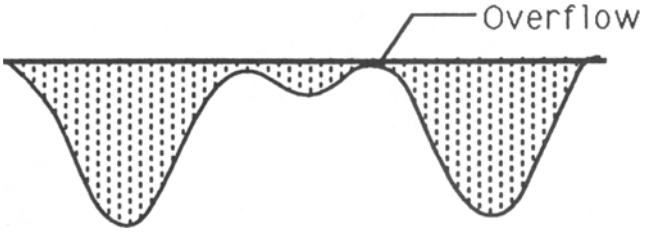

Fig. 21 Section of two engraved cells joined with a wall having a surface shape resulting from the overflow effect

Fig. 22 Shapes of the cells resulting from engraving at the different distances between the last lens and the roll surface with regard to the focus of this lens

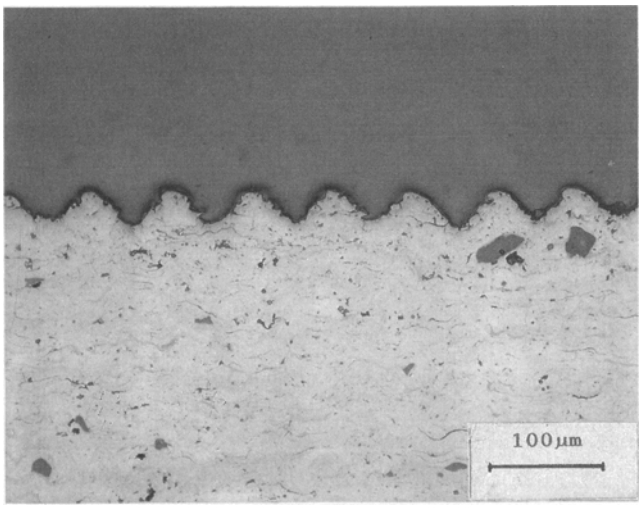

Fig. 23 Optical micrograph in bright field of the polished cross section of the coating deposited using A1 powder with the 1st set of spraying parameters (see Table 5). The coating was subsequently finished and treated using a Zedco engraver working with the 1st set of engraving parameters to achieve 140 1/cm LD and 34 μm cell depth (see Table 10).

Table 10 shows examples of engraving parameters that enable a demonstration of some of these effects.

4.2.4 Engraved Coating Examples

The roll, whose cross section is shown in Fig. 23, was sprayed with agglomerated A1 powder, and the spray parame-

ters (especially the high electric power) were well adapted to this powder of low apparent density. The sprayed coating, as expected, does not contain metallic inclusions, but the coating reveals poor contact between the lamellae. Some of them are visible inside the engraved cells.

Another roll, whose surface is shown in Fig. 24, was sprayed with fused and crushed (FC) powder and a custom-built plasma torch. This torch was supplied with low electric power (about 34 kW) and with a high working gas flow rate (70 NL/min of argon and 20 NL/min of hydrogen). This resulted in a plasma jet that had low enthalpy and, therefore, low ability to melt chromia particles. Chromia coatings sprayed under these conditions would contain many unmelted particles. Moreover, the unmelted or partially melted particles of high kinetic energy could easily rebound from the sprayed surface. As this coating was sprayed without any local aspirator, some of these could fall on the sprayed surface and become incorporated in the coating. At the deep engraving of 85 μm, the laser beam is coupled differently by the zone that includes the well-melted lamellae (left part in Fig. 24) and by the zone that includes a lot of unmelted ones (right part in Fig. 24). Finally, the engraved surface reveals inhomogeneity; see Fig. 24.

Figure 25 shows the surface of the ceramic anilox roll manufactured using correctly optimized parameters.

Table 10 Laser engraving parameters for several plasma-sprayed chromium oxide coatings

Engraving parameters	Set 1	Set 2
Roll dimensions (diameter × engraved length), mm	101 × 317	Diameter 70
Line density, 1/cm	140	60
Cell depth, μm	34	85
Engraving angle, degree	60	30
Surface speed, cm/s	30	18
Pulse length, μs	19	100
Pulse amplitude, %	99	90
Distance between last lens and coating surface(a), mm	50	...

Note: The Zedco Rapide engraver of ZED Instruments, London, England was used. (a) The focal distance of the last lens is 38 mm.

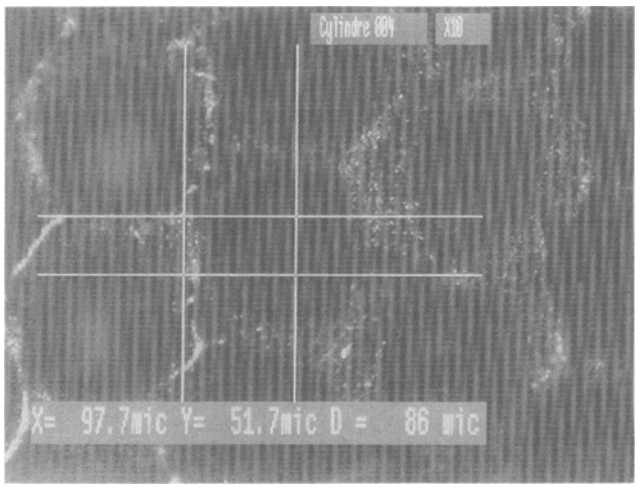

Fig. 24 Surface of the engraved roll showing nonhomogeneous cells The coating was deposited using FC powder with the 10th set of processing parameters (see Table 5). The coating was subsequently finished and treated using a Zedco engraver working with 2nd set of engraving parameters to achieve 60 1/cm LD and 85 μm cell depth (see Table 10)

4.3 *Postengraving Treatment*

The previously discussed effect of an overflow (see Fig. 21) can be reduced by polishing after engraving. The coating thickness to be taken off is no greater than a few micrometers. At the last stage, the engraved surface can be sealed with an epoxy resin thinned with acetone. The Auger electron spectroscopy (AES) technique established that the resin penetrates only a few micrometers into the coating (Ref 37).

5. Summary and Concluding Remarks

This technical review allows several conclusions with regard to anilox roll technology.

5.1 *Powders for Top Coatings*

The Cr_2O_3 composite powders with additives of SiO_2 and/or TiO_2 that are used at present for top coatings can be prepared with a greater weight fraction of additives than the present 5 wt%.

The fine (d_{50} about 10 μm) and "regular" (d_{50} about 30 μm) powders for top coating present deposits with properties that closely approach the specified values.

The Cr_2O_3 powder produced using fusing and crushing and sintering and crushing contained metallic chromium. These powders can result in a coating that does not follow the specifications. Thus the powders produced using fusing and sintering have to be carefully washed in acid to remove the metallic chromium. The crystalline and agglomerated powders can be readily used to spray the specified coatings.

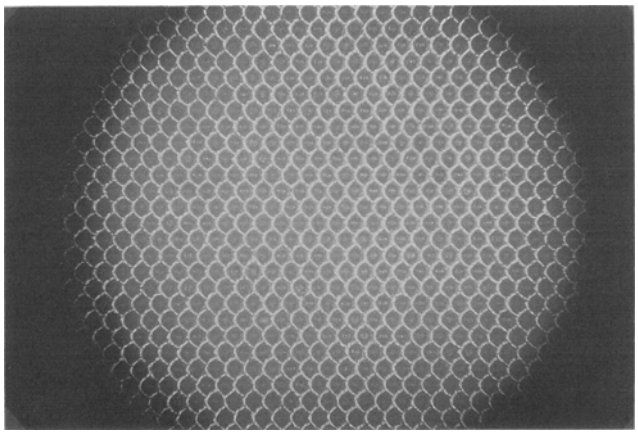

Fig. 25 Surface of a commercial ceramic anilox roll (reproduced with permission from Kurt Zecher GmbH, Paderborn, Germany)

5.2 *Thermal Spraying*

Powders manufactured using the agglomeration technique have to be sprayed using considerably greater electric power than for the other powders.

Application of oxygen as a carrier gas reduces oxygen loss during plasma spraying and renders top coatings more homogeneous.

Research concerning an analysis of the chromium oxide splat formation would enable better optimization of the processing parameters.

Modeling of heat penetration inside the porous, agglomerated particles in the plasma flame would permit better microstructure control.

Spraying time should be reduced. One method is spraying with a large powder feed rate using a highly powered torch (for example HEPS) accompanied by intense cooling (for example cryogenic cooling) of the coated substrate.

Tests of corrosion resistance of the duplex coatings (top coating onto bond coating) could be developed and adapted to the inks used in the anilox rolls service.

5.3 *Finishing*

The roughness of the top coating influences the depth of engraved cells. Thus a more systematic study of the influence of the top coating material and morphology on laser light absorption would enable quantification of the roughness of the top coating prior to laser engraving.

5.4 *Laser Engraving*

The ink transfer volume of laser engraved cells can be theoretically and experimentally determined for ceramic coatings. A theoretical study could relate the ink transfer with the cell shape, and the prediction could be verified by the experimental study of this parameter for typical inks. Moreover, the ink transfer volume could be related with the wetting angles of these inks onto the surfaces of coatings sprayed using different powders and finished to different roughnesses.

Standards for ceramic anilox roll line densities, angles, and depths should be formed. The standardization efforts would facilitate control of the roll quality and their production.

Acknowledgments

The author expresses gratitude to the company, W. Haldenwanger, Berlin, Germany, where he initiated the study of anilox rolls. The results of this study were not published, following mutual agreement, until two years after he left the company. The agglomerated powder tested in this study was manufactured with the help of Dr. Bartnik, Dr. Bialucki, and Dr. Kozerski of the Technical University of Wroclaw, Poland. The chromium oxide coatings were sprayed at W. Haldenwanger by Dipl. Ing. Hauff and Mr. Schneider; at Centro Sviluppo Materiali, Pergine, Italy by Mr. Zacchino, and at H.T.I., Ambazac, France by Mr. Bouleistaix. Some properties of the coatings were tested by Prof. Hildebrandt, T.U., Berlin, Germany; Dr. Kleinschrodt, B.A.M., Berlin, Germany; Dr. Zacchetti, C.S.M., Rome, Italy; and Dr. Sglavo, University of Trento, Italy. The laser engravings were carried out by ZED Instruments, London, England; Zecher, Paderborn, Germany; and Mr. Geneton, Cliche Bachkine, Limoges, France. Prof. Fauchais, University of Limoges, France kindly revised the manuscript and proposed the corrections that were later introduced to the text.

References

1. L. Pawlowski, R. Zacchino, R. Dal Maschio, V.M. Sglavo, J. Andresen, and F.J. Driller, Structure-Properties Relationship in Plasma Sprayed Chromium Oxide Coatings, *Thermische Spritzkonferenz TS93,* DVS-Berichte Band 152, DVS-Verlag GmbH, 1993, p 132-137
2. R. Douglas, Colour-Coded Ceramic, *Adv. Mater. Process.,* Vol 142 (No. 2), 1992, p 4
3. L. Pawlowski, *The Science and Engineering of Thermal Spray Coatings,* John Wiley & Sons, 1995
4. Z. Bartnik, P. Bialucki, S. Kozerski, P. Bork, B. Schrader, G. Clinton, K. Davies, F. Guglielmi, and L. Pawlowski, Improvements in Manufacturing Technology of Wear Resistant Plasma Sprayed Cr_2O_3 Coatings, *Thermal Spray: International Advances in Coatings Technology,* C.C. Berndt, Ed., ASM International, 1992, p 983-995
5. J. Beczkowiak and K. Mundinger, Quality Assurance during the Production of Fused Chromium Oxide, Characterization of the Powders and Properties of the Plasma Sprayed Coatings, *12th International Thermal Spraying Conference,* Paper 94, 4-9 June 1989, (London), The Welding Institute, 1989
6. S.J. Lukasiewicz, Spray-Drying Ceramic Powder, *J. Am. Ceram. Soc.,* Vol 72 (No. 4), 1989, p 617-624
7. L. Pawlowski and N. Zacchetti, Microstructural and Microanalytical Study of Cr_2O_3 Plasma Sprayed Coatings, *Advances in Inorganic Films and Coatings,* P. Vincenzini, Ed., Techna, 1995, p 381-390
8. Matthäus, OSU-Maschinenbau GmbH, Castrop-Rauxel, Germany, private information, 1992
9. L. Pawlowski, Optimisation of Arc Plasma Spraying Parameters, *Surfacing J.,* Vol 11 (No. 3), 1980, p 8-16
10. Fauchais, University of Limoges, France, private information, 1995
11. L. Pawlowski, A. Gross, and R. McPherson, Microstructure of Plasma Sprayed $YBa_2Cu_3O_x$ High-Temperature Superconductor, *J. Mater. Sci.,* Vol 26, 1991, p 3803-3808
12. Höhle, Sulzer-Metco (Deutschland) GmbH, Hattersheim, Germany, private information, 1995
13. M.I. Boulos, P. Fauchais, A. Vardelle, and E. Pfender, Fundamentals of Plasma Particle Momentum and Heat Transfer, *Plasma Spraying, Theory and Application,* R. Suryanarayanan, Ed., World Scientific, 1993, p 3-61
14. L. Pawlowski, The Properties of Plasma Sprayed Aluminium-Aluminium Oxide Cermets, *Surf. Coat. Technol.,* Vol 48, 1991, p 219-224
15. Emorine, Perkin Elmer Metco France, Argenteuil, France, private information, 1993
16. T. Cosack, L. Pawlowski, S. Schneiderbanger, and S. Sturlese, Thermal Barrier Coatings on Turbine Blades by Plasma Spraying with Improved Cooling, *37th ASME International Gas Turbine & Aeroengine Congress and Exposition,* Paper 92-GT-319, 1-4 June 1992, (Cologne, Germany), American Society of Mechanical Engineers
17. L. Pawlowski, Microstructural Study of Plasma Sprayed Alumina and Nickel Chromium Coatings, *Surf. Coat. Technol.,* Vol 31, 1987, p 103-116
18. J.M. Houben, "Relation of the Adhesion of Plasma Sprayed Coatings to the Process Parameters, Size, Velocity and Heat Content of the Spray Particles," Ph.D. thesis, Technical University of Eindhoven, 1988
19. L. Bianchi, F Blein, P. Lucchese, M. Vardelle, A. Vardelle, and P. Fauchais, Effect of Particle Velocity and Substrate Temperature on Alumina and Zirconia Splats Formation, *Thermal Spray Industrial Applications,* C C. Berndt and S. Sampath, Ed., ASM International, 1994, p 569-574

20. D. Grasme, Application of Water Stabilized Plasma Torch of 200 kW to Spray the Ceramic Coatings, *Thermische Spritzkonferenz TS 93,* DVS-Berichte Band 152, DVS-Verlag GmbH, 1993, p 14-18
21. L. Pawlowski, A. Hill, R. McPherson, D. Garvie, Z. Przelozny, and T. Finlayson, Properties of Plasma Sprayed $YBa_2Cu_3O_x$ High Temperature Superconductors, *Thermal Spray Research and Applications,* T.F. Bernecki, Ed , ASM International, 1990, p 641-646
22 C.W.D. Andrews, B.A, Fuller, and I. Preece, Observation of Arc-Plasma Sprayed Ferrite Films on Alumina Substrates, *J. Mater. Sci. Lett.,* Vol 9, 1974, p 856-858
23. G.M. Ingo, E. Parapazzo, O. Bagnarelli, and N. Zacchetti, XPS Studies on Cerium, Zirconium and Yttrium Valence States in Plasma Sprayed Coatings, *Surf. Interface Anal.,* Vol 16, 1990, p 515-519
24. G.M. Ingo, Origin of Darkening in 8 Wt.% Yttria-Zirconia Plasma Sprayed Thermal Barrier Coatings, *J. Am. Ceram. Soc.,* Vol 74, 1991, p 381-386
25. J.K. Niemi, P.M.J. Vuoristo, and T.A. Mäntylä, Chromium Oxide Coatings Deposited by Plasma Spraying and Detonation Gun Spraying, *2nd Plasma Technik Symposium Proceedings,* Vol 1, S. Blum-Sandmeier, H. Eschnauer, P. Huber, and A.R. Nicoll, Ed , Plasma-Technik AG, 1991, p 311-322
26. D. Gansert, E. Lugscheider, and U. Müller, High Power Plasma Spraying of Oxide Ceramics, *Thermal Spray Research and Applications,* T.F. Bernecki, Ed., ASM International, 1990, p 517-520
27 D. Chuanxian and H. Bingtang, Structure and Properties of Chromium Oxide Coatings, *Advanced Thermal Spraying Technology and Allied Coatings Symposium,* Sponsored by High Temperature Society of Japan, (Osaka, Japan), 13-15 May 1988, p 341-345
28. W. Funk, F. Goebe, and M. Mauz, The Influence of Substrate Temperature on the Bond Strength of Plasma Sprayed Oxide Ceramics, *1st Plasma Technik Symposium Proceedings,* Vol. 1, H. Eschnauer, P. Huber, A.R. Nicoll, and S. Sandmeier, Ed., Wohlen, Switzerland, 1988, p 59-66
29. C. Richard, J. Lu, J.F. Flavenot, G. Beranger, and F. Decomps, Study of Cr_2O_3 Coating Materials and Characterization by an Interfacial Test of Coating/Substrate Adherence, *Thermal Spray: International Advances in Coatings Technology,* C.C. Berndt, Ed., ASM International, 1992, p 11-16
30. A. Tronche and P. Fauchais, Hard Coatings (Cr_2O_3, WC-Co) Properties on Aluminium or Steel Substrates, *Mater. Sci. Eng.,* Vol 92, 1987, p 133-144
31. Catalogue of Pamarco Inc., Roselle, New Jersey, USA
32. Catalogue of Arc International, Charlotte, North Carolina, USA
33. Catalogue of Baasel-Scheel Lasergraphics GmbH, Itzehoe, Germany
34. Eschmeier, Windmöller & Hölscher, Langerich, Germany, private information, 1991
35. Engineering staff of Coherent Inc., *Lasers, Operation, Equipment, Application and Design,* McGraw-Hill, 1980
36. K. Davies, ZED Instruments, London, England, private information, 1992
37 Kleinschrodt, Bundesanstalt für Materialprüfung, Berlin, Germany, private information, 1988